Current Applied Physics 11 (2011) 933–938

Contents lists available at ScienceDirect

Current Applied Physics

journal homepage: www.elsevier.com/locate/cap

Synthesis and spectral properties of nanocrystalline Eu^{3+}-doped pyrochlore oxide $M_2Sn_2O_7$ (M = Gd and Y)

Zuoling Fu [a,b,*], Wangda Gong [a], Huaiyong Li [d], Qi Wu [a], Wenhao Li [c], Hyun Kyoung Yang [d], Jung Hyun Jeong [d,**]

[a] College of Physics, Jilin University, Key Lab of Coherent Light, Atomic and Molecular Spectroscopy, Ministry of Education, Changchun 130023, China
[b] State Key Laboratory of Superhard Materials, Jilin University, Changchun 130021, China
[c] Changchun Institute of Optics, Fine Mechanics and Physics, Chinese Academy of Sciences, Changchun 130033, China
[d] Department of Physics, Pukyong National University, Busan 608-737, Republic of Korea

ARTICLE INFO

Article history:
Received 28 December 2009
Received in revised form
31 August 2010
Accepted 27 December 2010
Available online 6 January 2011

Keywords:
Hydrothermal synthesis
Nanocrystalline
$M_2Sn_2O_7$ (M = Gd and Y):Eu^{3+}
Spectral properties

ABSTRACT

Nanocrystalline Eu^{3+}-doped pyrochlore oxide $M_2Sn_2O_7$ (M = Gd and Y) has been successfully prepared by a simple and facile hydrothermal synthesis method without the presence of catalysts. The effects of hydrothermal temperature, time and base concentration on the pure phase of the products are investigated. It is found that tuning the base concentration was a crucial step for the control of the pure phase of the $M_2Sn_2O_7$ (M = Gd and Y) nanocrystals. All the products were systematically characterized by powder X-ray diffraction (XRD), field emission-scanning electron microscopy (FE-SEM), transmission electron microscopy (TEM), Fourier-Transform Infrared Spectroscopy (FT-IR), photoluminescence (PL) and photoluminescent excitation spectra (PLE). Furthermore, the luminescence mechanism and size dependence of their spectral properties are also discussed in detail.

1. Introduction

Pyrochlore oxides are of importance in view of their catalytic activities and high-temperature stabilities in various reaction processes [1]. The basic framework of the pyrochlore structures is a three-dimensional corner-sharing network of MO_6 octahedra [2,3]. Recently, there has been a growing interest in strong luminescence of europium ions activated nanocrystals due to their promising applications in fluorescent lamps[4], field emission display[5] and plasma display panels[6]. $M_2Sn_2O_7$ stannates (M = rare earth) are conventionally prepared from solid state reactions at high temperatures ($\geq$1400 °C). Besides their high energy consumption, these solid state reactions involve a series of laborious heating cycles at high temperatures and repeated grinding of starting oxide components. The resulting powders show extensive agglomeration and compositional inhomogeneity. Therefore, there is a real need to develop an alternative synthesis route for pyrochlore stannates. Now, a few papers have been published on the preparation and properties of undoped $M_2Sn_2O_7$ stannates (M = rare earth) nanocrystals [7–9], but far fewer papers have been published on the synthesis and properties of lanthanide-doped $M_2Sn_2O_7$ stannates (M = rare earth) nanocrystals[10–12]. The hydrothermal synthesis technique [7,12] has been shown to be promising in the preparation of complex oxides in terms of the relatively low reaction temperatures employed, high quality of the crystals obtained and, in some cases, reduction in sizes of the particles of the product solids. In this paper, $M_2Sn_2O_7$:Eu^{3+} (M = Gd and Y) nanocrystals were prepared by hydrothermal synthesis method. The optimal synthesized conditions for $M_2Sn_2O_7$:Eu^{3+} (M = Gd and Y) nanocrystals were studied. Finally, the luminescent properties of bulk and nanocrystalline $M_2Sn_2O_7$:Eu^{3+} (M = Gd and Y) were investigated in detail.

2. Experimental sections

2.1. Preparation of $M_2Sn_2O_7$:Eu^{3+} (M = Gd and Y) nanocrystals

2.1.1. Materials

Yttrium nitrate hexahydrate ($Y(NO_3)_3 \cdot 6H_2O$), gadolinium nitrate hexahydrate($Gd(NO_3)_3 \cdot 6H_2O$), tin tetrachloride pentahydrate ($SnCl_4 \cdot 5H_2O$), europium nitrate pentahydrate ($Eu(NO_3)_3 \cdot 5H_2O$) and hydrazine monohydrate ($N_2H_4 \cdot H_2O$, 64–65%) were obtained from Aldrich. All of the chemicals were used without further purification. For the hydrothermal treatment, we used 80 mL Teflon cups.

* Corresponding author. College of Physics, Jilin University, Key Lab of Coherent Light, Atomic and Molecular Spectroscopy, Ministry of Education, Changchun 130023, China. Tel.: +86 431 85167966; fax: +86 431 85167966.
** Corresponding author.
E-mail addresses: zlfu@jlu.edu.cn (Z. Fu), jhjeong@pknu.ac.kr (J.H. Jeong).

1567-1739/$ – see front matter © 2010 Elsevier B.V. All rights reserved.
doi:10.1016/j.cap.2010.12.023

2.1.2. Synthesis

In a representative synthesis route, yttrium nitrate hexahydrate ($Y(NO_3)_3 \cdot 6H_2O$, 1.155 mmol), or gadolinium nitrate hexahydrate($Gd(NO_3)_3 \cdot 6H_2O$, 1.155 mmol), tin tetrachloride pentahydrate ($SnCl_4 \cdot 5H_2O$, 1.155 mmol) and europium nitrate pentahydrate ($Eu(NO_3)_3 \cdot 5H_2O$,0.035 mmol) were dissolved in 35 mL of deionized water and the mixture was stirred for 1 h. Then hydrazine monohydrate ($N_2H_4 \cdot H_2O$) acting as the mineralizer was added dropwise into the above solutions with different volume ratios. $N_2H_4 \cdot H_2O$ immediately reacted with $SnCl_4$ and rare earth nitrate solutions and a slurrylike white precipitate was formed. The mixture was stirred again for 2 h. Finally, the mixture was placed in a polytetrafluoroethylene (PTFE) vessel, and the vessel was capped by a PTFE cover and was placed inside a stainless steel autoclave. The autoclave was maintained at 200 °C for 24 h and cooled naturally to room temperature. The precipitate was filtered and washed with alcohol and deionized water several times. The precipitates were dried at 50 °C on air. The precursor powders were calcined at 900 °C for 3 h. Finally, the uniform distribution $M_2Sn_2O_7:Eu^{3+}$ (M = Gd and Y) nanocrystals were obtained.

In order to investigate the luminescent properties, bulk $M_2Sn_2O_7:Eu^{3+}$ (M = Gd and Y) powders were obtained by direct solid state reaction method. The starting materials were Y_2O_3, Gd_2O_3, SnO_2 and Eu_2O_3. According to the nominal compositions of compounds $M_2Sn_2O_7$: xEu^{3+} (M = Gd and Y; x = 0.03), the appropriate amount of starting materials were thoroughly mixed and ground then heated at 800 °C for 4 h. After being reground, they were calcined at 1500 °C for two days and regrinding at least two or three times. In addition, it should be mentioned that the activators content (Eu) was maintained at 3 mol % for the prepared samples.

2.2. Characterization

The structural characteristics of the bulk and nanocrystals $M_2Sn_2O_7:Eu^{3+}$ (M = Gd and Y) were measured from the X-ray diffraction (XRD) patterns using a Philips XPert/MPD diffraction system with Cu K_α (λ = 0.15405 nm) radiation and the Fourier-Transform-Near Infrared Spectrometer (FT-IR, Perkin Elmer(USA) Spectrum GX). The morphology and the size of the obtained samples were observed with field emission-scanning electron microscopy (FE-SEM, JSM-6700F, JEOL) and transmission electron microscopy (TEM, JEM-2010 JEOL). For the optical investigation, the photoluminescence (PL) and photoluminescence excitation spectra (PLE) measurements were obtained at room temperature by using a luminescence spectrometer (PTI, Time Resolved Fluorescence Meter) with Xe-lamp as an excitation source. The high-resolved emission spectra were detected by a Dye laser (Spectron Laser Sys. SL4000) pumped by the second harmonic (532 nm) of a pulsed Nd:YAG (yttrium aluminum garnet) laser (Spectron Laser Sys. SL802G).

3. Results and discussion

3.1. Synthesis and morphology of $M_2Sn_2O_7:Eu^{3+}$ (M = Gd and Y)

Fig. 1 shows the results of the XRD analysis of the calcined powders as a function of $N_2H_4 \cdot H_2O$ volume in the range of 2.5–5 ml. Suitable conditions for the synthesis of single phase crystalline $M_2Sn_2O_7:Eu^{3+}$ (M = Gd and Y) powders were investigated by varying such factors as the base ($N_2H_4 \cdot H_2O$) concentration, reaction temperature and time. $N_2H_4 \cdot H_2O$ acted as a mineralizer and played an important role in the syntheses of $M_2Sn_2O_7:Eu^{3+}$ (M = Gd and Y). Firstly, the only variable is the base concentration used for each reaction system. For example, at a $N_2H_4 \cdot H_2O$ volume of <3 ml in the Gd system, Gd_2O_3 was formed as impurity, whereas 4 ml $N_2H_4 \cdot H_2O$ led to the formation of SnO_2 as impurity; the suitable $N_2H_4 \cdot H_2O$ volume for the Gd and Y systems were *ca.* 3 and 3.5 ml, respectively. In these experimental ranges, no

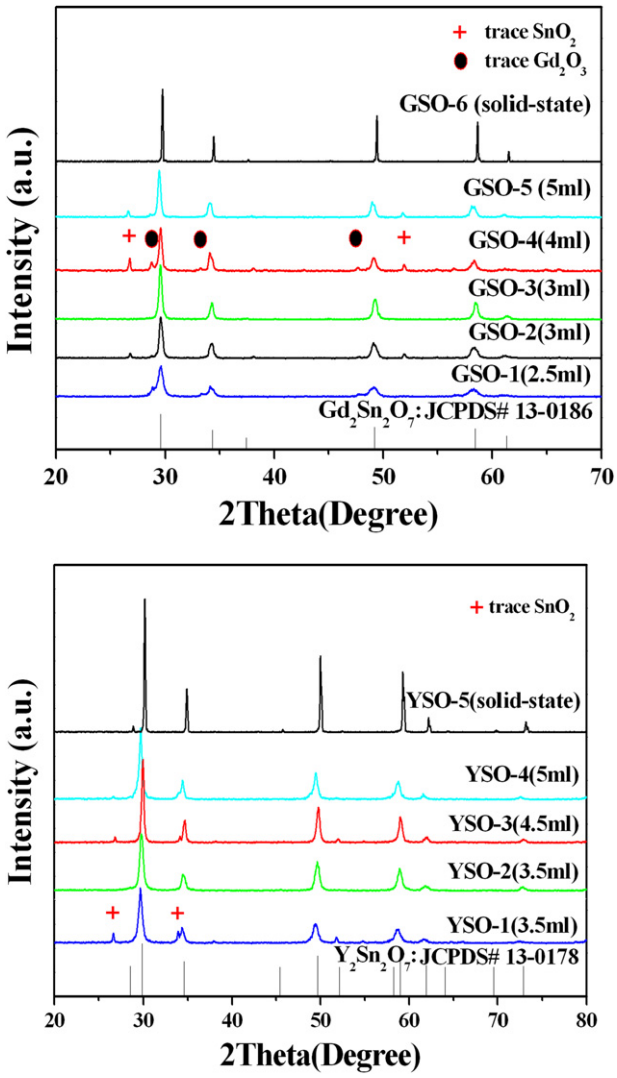

Fig. 1. XRD powder patterns of bulk and nanocrystalline $M_2Sn_2O_7:Eu^{3+}$ (M = Gd and Y) with different volume of $N_2H_4 \cdot H_2O$, reaction temperature and time. The detailed explanation is shown in Table 1.

impurity peaks were detected. All the peaks can be indexed to the cubic phase of $Gd_2Sn_2O_7$ and $Y_2Sn_2O_7$, which are in agreement with the standard data from JCPDS card No. 13-0186 and 13-0178, respectively. In general, the nanocrystallite size can be estimated from the Scherrer equation, $D = 0.89\lambda/\beta \cos\theta$, where D is the average

Table 1
The synthesis conditions for bulk and nanocrystalline $M_2Sn_2O_7:Eu^{3+}$ (M = Gd and Y).

Samples	Volume $N_2H_4 \cdot H_2O$/ml	Of temperature/°C	Time/hours	Phase(s) in product
YSO-1	3.5	200	12	$SnO_2 + Y_2Sn_2O_7$
YSO-2	3.5	200	24	$Y_2Sn_2O_7$
YSO-3	4.5	200	24	$SnO_2 + Y_2Sn_2O_7$
YSO-4	5	200	24	$SnO_2 + Y_2Sn_2O_7$
YSO-5	-	1500	10	$Y_2Sn_2O_7$
GSO-1	2.5	200	24	$Gd_2O_3 + Gd_2Sn_2O_7$
GSO-2	3	180	24	$SnO_2 + Gd_2Sn_2O_7$
GSO-3	3	200	24	$Gd_2Sn_2O_7$
GSO-4	4	200	12	$SnO_2 + Gd_2O_3 + Gd_2Sn_2O_7$
GSO-5	5	200	24	$SnO_2 + Gd_2O_3 + Gd_2Sn_2O_7$
GSO-6	-	1500	10	$Gd_2Sn_2O_7$

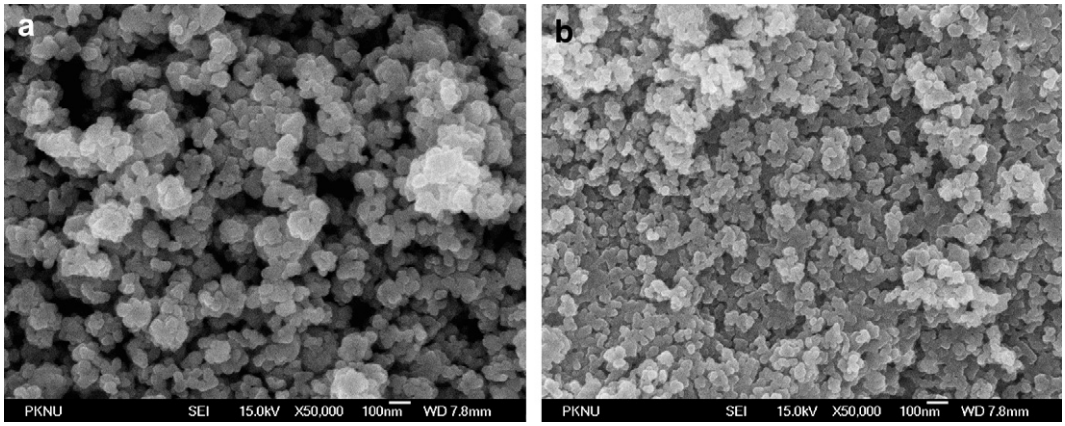

Fig. 2. FE-SEM images of $Gd_2Sn_2O_7:Eu^{3+}$ (a) and $Y_2Sn_2O_7:Eu^{3+}$ (b) nanocrystals.

crystallite size, λ is the X-ray wavelength (0.15405 nm), and θ and β are the diffraction angle and full-width at half-maximum (in radian) of an observed peak, respectively. The estimated average crystallite sizes are about 42 and 28 nm for GSO-3 and YSO-2, respectively.

In addition, the reaction temperature and time also influenced the formation of products. When the temperature is at 180 °C, however, we can not obtain the pure phase (GSO-2). While the time is shorter than 24 h, we also can not obtain the pure phase (YSO-1). Therefore, a crystallization temperature of 200 °C and a crystallization time of 24 h were optimal. All the synthesis conditions for the bulk and nanocrystalline $M_2Sn_2O_7:Eu^{3+}$ (M = Gd and Y) were listed in Table 1. Fig. 2(a) and (b) presents typical FE-SEM images of nanocrystalline $M_2Sn_2O_7:Eu^{3+}$ (M = Gd and Y) after annealed at 900 °C. For the $M_2Sn_2O_7:Eu^{3+}$ (M = Gd and Y) nanocrystals, all the particles are regular and uniform, which are also confirmed by TEM (Fig. 3(a) and (b)).The particle sizes were estimated about 50 and 30 nm for GSO-3 and YSO-2 nanocrystals, respectively, which are consistent with the calculated sizes by the Scherrer equation.

It has been reported that pyrochlore oxides exhibit seven IR bands in the range of 750–50 cm^{-1} originating from vibration and bending of metal-oxygen bonds [1]. However, it is impossible to report IR spectra below 500 cm^{-1} with our instrument. The effect of the cation and particle size was evident in the FT-IR spectra of $M_2Sn_2O_7:Eu^{3+}$ (M = Gd and Y), as shown in Fig. 4. All spectra show one broad band due to M-O-Sn vibrations which shift progressively to higher wavenumbers, as a consequence of differences in ionic size from Gd(1.078Å) to Y(1.040Å) [7]. Basically three factors seem to influence the location of the band maxima: (i) radius of the M^{3+} ions, (ii) the mass of the M element and (iii) the occurrence of the M element in Group III_a or III_b(Ln's). It is as expected that the high frequency band (520–575 cm^{-1}) is in direct proportion to the crystallographic lattice parameter (and hence the unit cell volume) a in the pyrochlores and as a decreases, the bond strength increases [13]. However, in this case, compared with that of bulk materials, the IR absorption bands in nanocrystals shift to higher wavenumbers with the decease of particles size, which could result from somewhat different chemical environment.

3.2. Spectral analysis of bulk and nanocrystalline $M_2Sn_2O_7:Eu^{3+}$ (M = Gd and Y)

Fig. 5 shows representative room temperature photoluminescence excitation (PLE) spectra of bulk and nanocrystalline $M_2Sn_2O_7:Eu^{3+}$ (M = Gd and Y). The excitation spectrum exhibits broad band between 200 and 300 nm, which can be attributed to charge transfer band between the Eu^{3+} and the surrounding oxygen anions [14–16]. The excitation peaks of bulk $Gd_2Sn_2O_7:Eu^{3+}$ and $Y_2Sn_2O_7:Eu^{3+}$ are centered at 274 and 270 nm, respectively, indicative of a blue-shift orientation when M^{3+} is changed from Gd^{3+} to Y^{3+}; As reported, CTB is strongly related to the covalency between O^{2-} and Eu^{3+} [17,18]. In the bond structure of $Eu^{3+}-O^{2-}-M^{3+}$ (M = Gd and Y), the degree of covalency of the $Eu^{3+}-O^{2-}$ bond is weaker in the $Y_2Sn_2O_7$ structure because Y^{3+} attracts electrons of O^{2-} most strongly due to the fact that it has the larger electronegativity and the smaller radius [17,18]. Therefore, it could be easier for the electronic transition from the 2p orbital of O^{2-} to the 4f orbital of Eu^{3+} in the $Gd_2Sn_2O_7$ host than in the

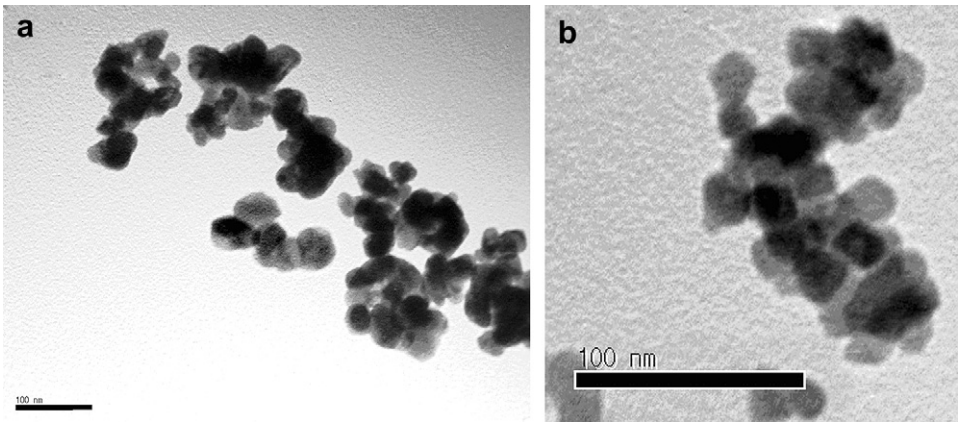

Fig. 3. TEM micrographs of $Gd_2Sn_2O_7:Eu^{3+}$ (a) and $Y_2Sn_2O_7:Eu^{3+}$ (b) nanocrystals.

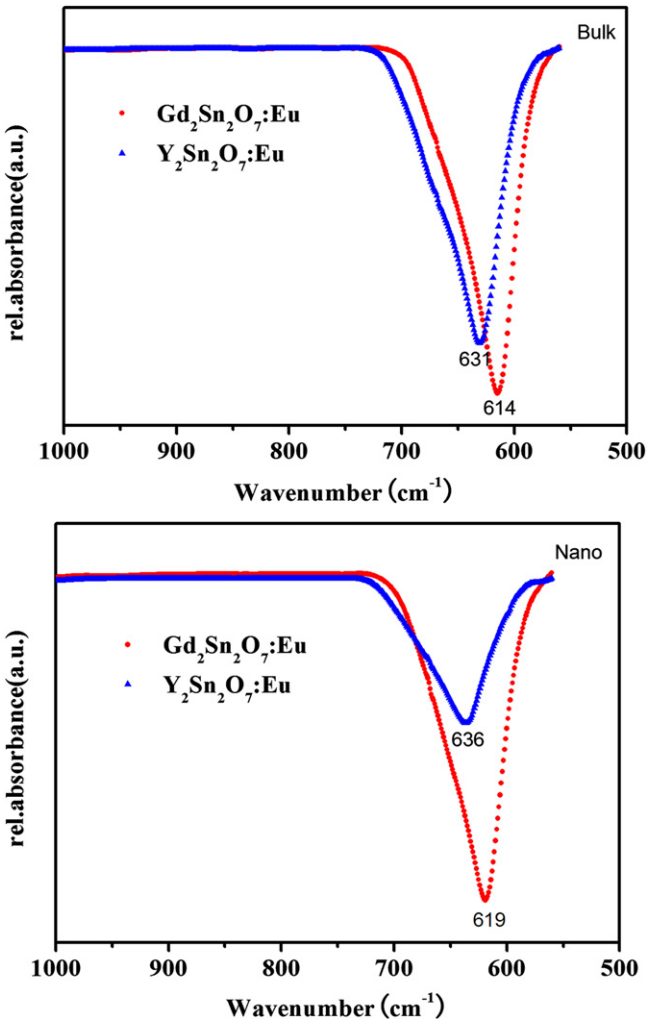

Fig. 4. FT-IR spectra of $Gd_2Sn_2O_7$:Eu^{3+} (a) and $Y_2Sn_2O_7$:Eu^{3+} (b) nanocrystals.

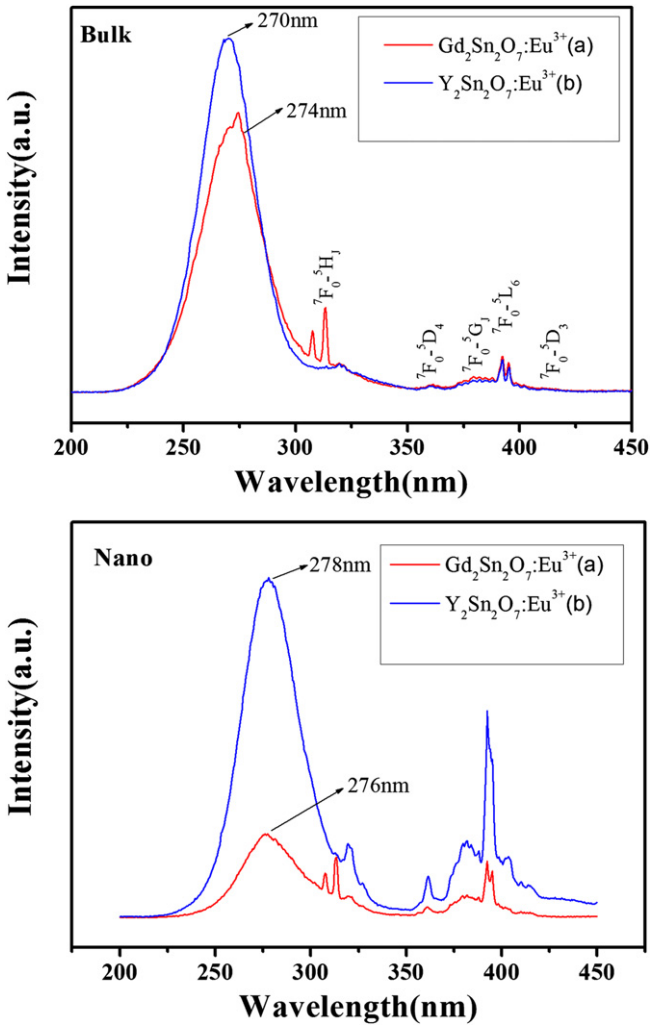

Fig. 5. PLE spectra of bulk and nanocrystalline $Gd_2Sn_2O_7$:Eu^{3+}(a); $Y_2Sn_2O_7$:Eu^{3+} (b)for the emission at 587 and 589 nm, respectively.

$Y_2Sn_2O_7$ one, and thus the CTB energy of Eu^{3+} decreases in the series of Y^{3+} to Gd^{3+} stannate phosphors.

The PLE spectra of nanocrystalline $M_2Sn_2O_7$:Eu^{3+} (M = Gd and Y) were shown in Fig. 5(Nano). Compared with that of the corresponding bulk materials, the excitation bands of nanocrystalline $M_2Sn_2O_7$:Eu^{3+} (M = Gd and Y) show obvious red shift, which is responsible for the change of the unit cell parameters in Table 2. For nanocrystalline $M_2Sn_2O_7$:Eu^{3+} (M = Gd and Y), the unit cell parameters increase with the particle size decrease, so Eu^{3+}–O^{2-} bond length becomes longer in nanocrystals. The degree of covalency of the Eu^{3+}–O^{2-} becomes stronger in the nanocrystalline $M_2Sn_2O_7$:Eu^{3+} (M = Gd and Y). Therefore, the CTB energy of Eu^{3+} in nanocrystals located in lower energy, which is in good agreement with the rule in the bulk CTB energy change from Y to Gd.

It is well-known that the chromaticity of the emission from the Eu^{3+} ions depends on the local symmetry due to the transition rules described in terms of Judd–Ofelt theory [19]. When the Eu^{3+} ions locate in the sites with the inversion center, the orange emissions become relatively strong, while the red emissions become very weak because electronic dipole transitions are parity forbidden. If the lattice around Eu^{3+} ions is distorted, their local symmetry deviates from the inversion center, which allows red emissions. Pyrochlore has a face-centered cubic structure (space group Fd3m) with eight formula units per conventional unit cell [20]. In the ideal $A_2B_2O_7$ pyrochlore structure the A site is a distorted cube and the B site is regular octahedron [21]. The coordination is 8-fold for the A site and 6-fold for the B site. In $M_2Sn_2O_7$, therefore, M^{3+} and Sn^{4+} are surrounded by eight and six oxygen ions, respectively. Because eight oxygen ions form a distorted cube, the M^{3+} site symmetry is lowered to D_{3d} [22]. The charge and ionic radii of Eu^{3+} (1.066 Å for the coordination number of 8) would prefer substitution for M^{3+} rather than for Sn^{4+} (0.69 Å) in the $M_2Sn_2O_7$ lattice. Fig. 6 displays the PL spectra in bulk and nanocrystalline $M_2Sn_2O_7$:Eu^{3+} (M = Gd and Y). Assuming that Eu^{3+} is located at the site with D_{3d} symmetry, the enhanced and sharpened $^5D_0$-$^7F_1$ emissions of Eu^{3+} in the nanocrystalline $M_2Sn_2O_7$(see Fig. 6(Nano) host crystal can be reasonably explained by the allowed magnetic–dipole transition due to the presence of an inversion center. Nevertheless, the split $^5D_0$-$^7F_2$ emissions coexist in the spectra even for the highly crystalline $M_2Sn_2O_7$:Eu^{3+} that was

Table 2
Unit cell parameters for $M_2Sn_2O_7$:Eu^{3+} (M = Gd and Y) bulk and nanocrystalline samples.

Sample	a(Å)	Std. error for a (Å)	Cell volume ($Å^3$)
JCPDS#13-0086 ($Gd_2Sn_2O_7$)	10.460		1144.4
GSO-6 (Bulk)	10.417	±0.0061	1130.4
C-SO-3 (Nano)	10.464	±0.0022	1145.7
JCPDS 13-0078 ($Y_2Sn_2O_7$)	10.371		1115.5
YSO-5 (Bulk)	10.327	±0.0076	1101.3
YSO-2 (Nano)	10.393	±0.0024	1122.7

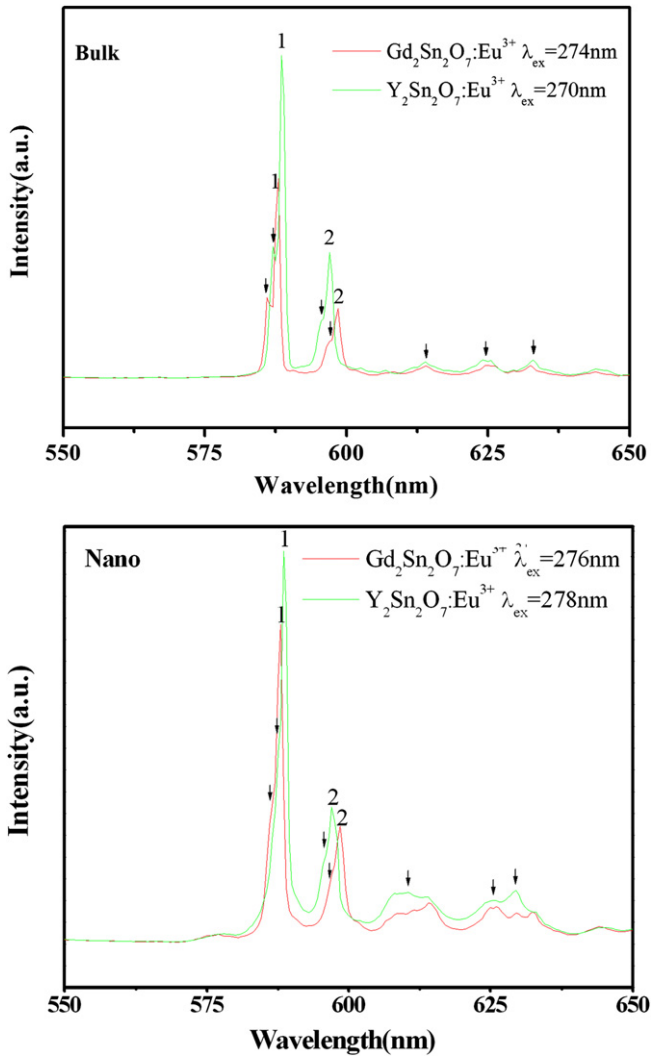

Fig. 6. PL spectra of bulk and nanocrystalline $Gd_2Sn_2O_7:Eu^{3+}$ and $Y_2Sn_2O_7:Eu^{3+}$ for the excitation at 274, 276, 270 and 278 nm, respectively.

heated at 1500 °C see Fig. 6(Bulk)). It might be regard that a local distortion of the crystal field might be produced in bulk and nanocrystals, reducing the symmetry of crystal field surrounding the Eu^{3+} activator, and then red emissions are allowed. Therefore, the peaks labeled by arrow in PL spectra could be relation to the lattice distortion.

The $^5D_0$-$^7F_1$ transitions of the Eu^{3+} ions were split into two lines (1 and 2), indicating that the Eu^{3+} ions were located in the site with D_{3d} symmetry. The peak wavelengths of the $^5D_0$-$^7F_1$ transitions (λ_1 and λ_2) and splitting widths ($\Delta\lambda = \lambda_1$-$\lambda_2$) for bulk and nanocrystalline $M_2Sn_2O_7:Eu^{3+}$ (M = Gd and Y) are summarized in Table 3. For the same kind of materials between the bulk and nanocrystals, no

Table 3
Peak wavelengths of the $^5D_0$-$^7F_1$ transition of $M_2Sn_2O_7:Eu^{3+}$ (M = Gd and Y) bulk and nanocrystalline samples.

Sample	Peak wavelengths nm		Splitting width
	λ_1	λ_2	$(\Delta\lambda)/cm^{-1}$
GSO-6 (Bulk)	588	598	285
GSO-3 (Nano)	588	598	285
YSO-5 (Bulk)	589	597	228
YSO-2 (Nano)	589	597	228

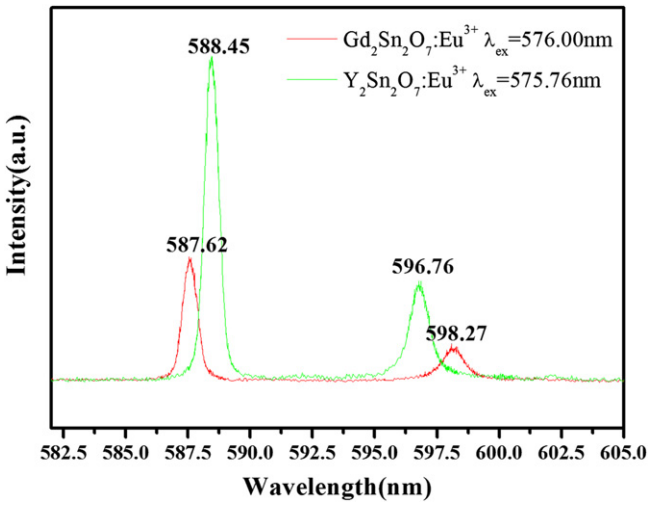

Fig. 7. High-resolved emission spectra of bulk $Gd_2Sn_2O_7:Eu^{3+}$ and $Y_2Sn_2O_7:Eu^{3+}$ for the excitation at 576.00 and 575.76 nm, respectively.

obvious change for the splitting widths was observed. However, significant change was observed for the splitting widths between $Y_2Sn_2O_7:Eu^{3+}$ and $Gd_2Sn_2O_7:Eu^{3+}$.The high-resolved emission spectra of bulk $M_2Sn_2O_7:Eu^{3+}$ (M = Gd and Y) were also shown in Fig. 7. The splitting widths in $Gd_2Sn_2O_7:Eu^{3+}$ system is larger than that in $Y_2Sn_2O_7:Eu^{3+}$, which suggested that the crystal field strength in $Gd_2Sn_2O_7:Eu^{3+}$ is stronger than that in $Y_2Sn_2O_7:Eu^{3+}$. This is consistent with the observed results of CTB in $M_2Sn_2O_7:Eu^{3+}$ (M = Gd and Y). The centre energy is higher, the crystal field strength is stronger, the CTB should locate in lower energy. McCauley and Humnel [23] reported that larger distortion of EuO_8 scalenohedra induces larger splitting widths of the $^5D_0$-$^7F_1$ transitions of Eu^{3+} ions in $A_2B_2O_7$(A = La, Gd, Y, Lu; B = Ti, Zr, Sn) pyrochlores.

4. Conclusion

$M_2Sn_2O_7:Eu^{3+}$ (M = Gd and Y) nanocrystals have been successfully synthesized by a hydrothermal process followed further calcining treatment. Suitable conditions for the synthesis of single phase $M_2Sn_2O_7:Eu^{3+}$ (M = Gd and Y) nanocrystals were a crystallization temperature of 200 °C and a crystallization time of 24 h. Repetitions experiments confirmed that this method was not only simple but also quite effective. Compared with that of bulk materials, the IR absorption bands in nanocrystals show a small shift, which results from somewhat different chemical environment. The CTB energy of Eu^{3+} in nanocrystals located in lower energy, which is in good agreement with the rule in the bulk CTB energy change from Y to Gd. PL spectra indicated the occurrence of the orange and red luminescence at a single-wavelength excitation due to the doubly split $^5D_0$-$^7F_1$ and $^5D_0$-$^7F_2$ transitions, which could be relation to the lattice distortion surrounding the Eu^{3+} activator.

Acknowledgments

This work was supported by the Fundamental Research Funds for the Central Universities (no. 421060551411), partially supported by a grant-in-aid for the National Science Foundation of China (no. 11004081) and by the Korea Research Foundation Grant funded by the Korean Government (2010-0022540) and by the National Core Research Center Program from MEST and NRF (2010-0001-226).

References

[1] M.A. Subramanian, G. Aravamuclan, G.V. Subba Rao, Prog. Solid State Chem. 15 (1983) 55.
[2] J.N. Reimeis, J.E. Greedan, J. Solid State Chem. 72 (1998) 390.
[3] H. Mizoguchi, H.W. Eng, P.M. Woodward, Inorg. Chem. 43 (2004) 1667.
[4] S.W. Kang, J.S. Yoo, J.D. Lee, J. Electrochem. Soc. 145 (1998) 648.
[5] D.K. Wilams, B. Bhihari, B.M. Tissue, J. Phys. Chem. B 102 (1998) 916.
[6] O.A. Serra, S.A. Cicillini, R.R. Jshiki, J. Alloys. Compound 303-304 (2000) 316.
[7] Y.C. Mao, G.S. Li, W. Xu, S.H. Feng, J. Mater. Chem. 10 (2000) 479.
[8] S.M. Wang, G.J. Zhou, M.K. Lu, Y.Y. Zhou, Z.S. Yang, J. Alloy. Compound 424 (2006) L3.
[9] J. Zeng, H. Yang, Y.C. Zhang, M.K. Zhu, H. Yan, J. Phys. Chem. C 111 (2007) 11879.
[10] Z.G. Lu, J.W. Wang, Y.G. Tang, Y.D. Li, J. Solid State Chem. 177 (2004) 3075.
[11] H. Cheng, L.P. Wang, Z.G. Lu, Nanotechnology 192 (2008) 025706.
[12] K.W. Li, H.L. Li, H.M. Zhang, R. Yu, H. Wang, H. Yan, Mater. Res. Bull. 41 (2006) 191.
[13] C.P. Poole, J.J. Owens, Introduction to Nanotechnology. John Wiley and Sons, Inc., Hoboken, New Jersey, 2003.
[14] R. Schmechel, M. Kennedy, H.V. Seggern, H. Winkler, M. Kolbe, R.A. Fischer, X.M. Li, A. Benker, M. Winterer, H. Hahn, J. Appl. Phys. 89 (2001) 1679.
[15] G. Blasse, B.C. Geiabmaier, Luminescent Materials. Springer, Berlin, 1994.
[16] G. Wakefield, E. Holland, P.J. Dobson, J.L. Hutchison, Adv. Mater. 13 (2001) 1557.
[17] G. Blasse, J. Chem. Phys. 45 (1966) 2356.
[18] G. Blasse, J. Chem. Phys. 51 (1969) 3529.
[19] R. Reisfeld, C.K. Jorgensen, Lasers and Excited States of Rare Earths. Springer, Berlin, 1977.
[20] Y.M. Jana, A. Sengupa, D.J. Ghosh, Magn. Magn. Mater. 248 (2002) 7.
[21] W.R. Panero, L. Stixrude, R.C. Ewing, Phys. Rev. B 70 (2004) 054110.
[22] E. López-Navarrete, V.M. Orera, F.J. Lazaro, J.B. Carda, M. Ocana, J. Am, Ceram. Soc. 87 (2004) 2108.
[23] R.A. McCauley, F.A. Hummel, J. Lumin. 6 (1973) 105.